Scalable synthesis of CO_2-selective porous single-layer graphene membranes

Jian Hao, Piotr Mieczyslaw Gebolis†, Piotr Marcin Gach, Mojtaba Chevalier, Luc Sébastien Bondaz, Kuang-Jung Hsu, Kapil Bhorkar, Deep J. Babu‡, and Kumar Varoon Agrawal*

Laboratory of Advanced Separations (LAS), École Polytechnique Fédérale de Lausanne (EPFL), 1950 Sion, Switzerland

†Present address: Tetra Pak eBeam Systems AG, 3175 Flamatt, Switzerland

‡Present address: Department of Materials Science and Metallurgical Engineering, Affiliated faculty – Dept. of Climate Change, Indian Institute of Technology Hyderabad, Kandi, Sangareddy, Telangana 502284, India

Abstract

Membranes based on atom-thin, porous single-layer graphene (PG) have shown attractive performance for diverse separation applications, especially gas separation and carbon capture. However, despite a decade of research, a scalable synthesis of PG membranes has remained under question. This is mainly because the literature resorts to complicated and expensive methods that yield small membranes and limited reproducibility. Herein, we introduce several interventions that significantly reduce PG membrane cost, allow uniform pore formation in a large area, and enable the preparation of large-area PG membranes with attractive performance. We show that mass transfer of the oxidant, neglected in the literature, plays a crucial role in achieving uniform oxidation of large-area graphene. Crack formation during the transfer of graphene, a major challenge in this field that also limits reproducibility, is eliminated using a novel protocol that does not require delicate floating and handling of graphene, allowing the realization of a high-performance 50 cm^2 graphene membrane in a cross-flow module.

Nanoporous atomically thin membranes (NATM) have emerged as a promising platform for effectively separating molecules and ions, exploiting mass, size, and affinity differences.[1–5] Despite significant progress on the fundamental aspects of NATM including transport mechanism, pore incorporation, and membrane fabrication, this field faces an outstanding critical challenge on the scalability of NATM membranes. The most popular and studied NATM is PG. Successful incorporation of carbon dioxide (CO_2)-selective pores in PG has led to attractive performance for carbon capture.[2,6–8] This involves selective separation of CO_2 from nitrogen (N_2). It is crucial to develop high-performance carbon capture membranes that reduce the consumption and the associated cost of carbon capture from point-emission sources. Indeed, technoeconomics assessments of the capture process based on high-performance PG membranes indicate that the energy efficiency of capture can be significantly improved compared to the commercial amine-based absorption process.[9,10] This is mainly because the membrane processes do not require thermal energy but rather rely on electrical energy.[11,12] This is also because PG membranes yield extremely high CO_2 permeance thanks to its atom-thin selective layer. This minimizes the required membrane area and the capture process footprint, making capture based on PG membranes advantageous compared to the state-of-the-art membranes based on polymers,[13,14] zeolites,[15,16] metal-organic frameworks,[17,18] covalent-organic frameworks,[19,20] and carbon molecular sieves.[21,22] A low-footprint capture process is attractive to application in the transportation sector, especially the international shipping industry, responsible for 2-3% of global CO_2 emissions.

The proof of concept study on the selective transport of CO_2 from PG was demonstrated by Bunch and coworkers in 2012.[2] This was a fundamental study from a micron-sized exfoliated graphene with only a couple of pores responsible for gas transport. However, for practical membranes, one must prepare macroscopic films. For this, polycrystalline graphene, produced by chemical vapor deposition (CVD) on Cu foil, has become a standard material.[23–25] Yet, it is challenging to prepare a large-area PG membrane. Several aspects of the PG membrane must be debottlenecked to become commercially attractive for carbon capture. This includes reducing membrane element cost, scalable incorporation of CO_2-selective pores in graphene, and crack-free fabrication of membranes. These challenges are elaborated below.

Currently, the cost of graphene membranes is prohibitively high. The literature uses extremely expensive Cu foils (500-10000 \$/m^2), manufactured by delicate processing, to prepare high-quality graphene for membrane application.[6,23,26] This high raw material cost is prohibitive for the carbon

capture application. For comparison, polymeric membranes for carbon capture have a membrane element cost of 20-50 $/m^2$.[27,28] Incidentally, the major cost of CVD graphene is related to the expensive Cu foil. However, Cu foils are also produced cheaply (~10 $/m^2$). An important challenge here is that low-cost Cu foils have surface imperfections in the form of micrometer-sized particles and large grooves and scratches. These imperfections are detrimental to the fabrication of high-quality graphene membranes for carbon capture because they compromise the integrity of the suspended graphene by generating cracks.[6,29,30]

The second challenge concerns the lack of demonstration of CO_2-selective pore incorporation in graphene over a large area. Pores in graphene are carbon vacancy defects incorporated by removing atoms from the basal plane. Chemical routes involving the gasification of the lattice by oxidation are intrinsically more scalable than carbon knockout routes using energetic beams. For oxidation, oxidative plasma,[31] oxygen (O_2),[32,33] ultraviolet light/ozone (O_3),[30] or O_3[8,34] have been demonstrated. However, they involved sophisticated setups that are challenging to scale up. The uniformity of pore incorporation over a large area is not demonstrated.

The third challenge relates to fabricating large-area PG membranes while avoiding cracks in graphene. Cracks typically manifest during the transfer of CVD graphene from the Cu foil to porous support or during pressurization of the PG membrane. Wafer-scale[23] and roll-to-roll[25,35] transfer have been demonstrated in fabricating graphene devices for electronic applications. However, while these applications are tolerant to macroscopic cracks in graphene, gas separation membranes are not. Crack-free PG is essential for selective transport between similar-sized gas molecules such as CO_2 and N_2 under pressurized conditions. Centimeter-scale PG membranes have been demonstrated for nanofiltration after stitching cracks using interfacial polymerization.[30,35,36] However, this approach has not been demonstrated for gas separation. We have shown that cracks in PG can be avoided by using gas-permeable mechanically reinforcing support film (MRF). Typically, MRF is deposited on PG, and the Cu foil is removed by wet-chemical etching, after which the floating composite PG/MRF is scooped on the desired porous support.[23,37–39] MRF can be a nanoporous carbon (NPC) film,[6] highly permeable polymers such as poly[1-(trimethylsilyl)-1-propyne] (PTMSP),[7] polydimethylsiloxane (PDMS),[40] or a composite film such as multi-walled carbon nanotube (MWCNT) deposited on NPC.[41] However, the success rate of achieving selective membranes (defined as the number of selective membranes normalized by the number of attempts) remains low (10-20%). This is mainly because the transfer protocol involves floating and scooping

steps where cracks can easily develop in PG. Transfer methods involving careful scooping of floating PG are also extremely challenging to scale up. Therefore, a key challenge is to develop a membrane fabrication route avoiding careful scooping of graphene and where the success rate is nearly 100%.

Herein, we present several advances towards scaling up PG membranes for carbon capture. We demonstrate the successful use of a low-cost Cu foil (10 \$/m^2) to prepare PG membranes with attractive CO_2/N_2 separation performance with a near 100% success rate. A simple protocol was developed to eliminate large contaminant particles on the surface of low-cost Cu foil. A large reactor for pore incorporation was implemented, which allowed the incorporation of uniform pores in large-area graphene (500 cm^2) in a reproducible manner. A systematic study of graphene oxidation revealed that O_3 mass transfer (velocity), as opposed to reaction kinetics (temperature and time), which has been the focus of the literature, dominates pore formation kinetics. A facile and user-friendly transfer protocol was developed, completely avoiding the floating step, resulting in a highly reproducible synthesis. These interventions yielded attractive performance with a near 100% success rate from PG membranes.

Results

High-quality graphene from low-cost Cu foil

For synthesizing high-quality large-area graphene on a low-cost Cu foil, a CVD system consisting of a 160 cm long furnace with a uniform heating zone of 110 cm, a gas delivery, and a pressure management subsystem was developed (**Figure 1a, b, Figure S1**). Two dumbbell-shaped blocks made of Cu are placed at the end of the reactor as radiation shields to prevent excessive heating of flanges sealing the reactor. Two large coupons of Cu foils, each with a size of 11 × 26 cm^2, could be introduced for graphene synthesis (**Figure 1c**).

Imperfection in Cu foil consists of surface contaminations (particles) and grooves. High-purity, expensive Cu foils have a low concentration of particles and have been reported to synthesize graphene after simple solvent washing. They are also free of large grooves and scratches. However, their cost is prohibitive for membrane application (**Table S1**). For low-cost Cu, contamination particles are present on the surface of the Cu foil and are likely deposited during the process of rolling Cu foils. Another source of contamination, irrespective of Cu foil, is the reaction between Cu vapor and the reactor wall made of a fused quartz tube, where SiO_x particles are formed. These

particles eventually deposit on the Cu foil, affecting graphene quality (**Figure S2a**).[42] These could be largely eliminated by placing a high-purity (99.7%) alumina tube (ϕ16 cm) inside the quartz tube, which screened off the quartz tube from Cu vapor (**Figure 1d**).[6,7,41,43]

We chose a low-cost Cu foil (10 $/m^2 at scale, **Table S1**) and developed a simple protocol for removing contamination, grooves, and scratches. Micron-sized particles formed by several elements (Ca, K, Al, or Cl) could be observed on the as-received Cu foils (**Figure S2b**). A facile protocol involving submerging Cu foil in a dilute nitric acid solution was developed. Dissolution of the Cu surface in the nitric acid effectively detached the particles from the surface of the Cu foil. An underlying challenge here is a tradeoff between removing particles and pittings of Cu foil as a function of treatment time and acid concentration. A treatment time of 10 min and an acid concentration of 4 wt% were found to be optimal. Scanning electron microscopy (SEM) based mapping of a relatively large area (~0.2 mm^2, **Figures S3, S4**) of graphene was used to analyze the particle density on the surface (**Figure 1e-h**). Acid treatment significantly reduced the density of particles. The population of particles smaller than 1 μm was reduced by 70%. Importantly, particles larger than 1 μm were eliminated. This is crucial for reducing cracks during graphene transfer because the macroscopic particles lead to pinhole defects during transfer. The acid treatment also smoothened grooves and scratches on the Cu foil. Optical microscopy images (**Figure 1i-l**) and profilometry mapping analysis (**Figure 1m, n, Figure S5**) demonstrate that graphene produced on acid-treated Cu foil has a significantly lower root mean square (RMS) surface roughness (150 nm) compared to that on as-received Cu foil (261 nm). Therefore, the two interventions, namely acid pretreatment and using the alumina tube in the CVD reactor, effectively reduced the surface contamination of graphene.

As-synthesized graphene was characterized by Raman spectroscopy. **Figure 1o** shows a spectrum where the two characteristic peaks of graphene, *G,* and *2D*, could be observed at 1589 and 2678 cm^{-1}, respectively. The *D* peak at ~1350 cm^{-1}, attributed to lattice defects, was negligible, confirming that high-quality graphene can be synthesized on a low-cost Cu foil. A *2D/G* peak intensity ratio of ~2.6 confirms that the graphene was a single layer. High-resolution aberration-corrected transmission electron microscopy (AC-HRTEM) further confirmed that graphene was a single layer (**Figure 1p**). Raman mappings (48 × 80 μm^2 area) of peak intensity ratio for *D*/*G* (I_D/I_G: 0.05±0.02, **Figure 1q**) and *2D*/*G* (I_{2D}/I_G: 2.15±0.35, **Figure 1r**) confirmed uniformity at

this length scale. Characterization of graphene at several locations along the 55 cm long synthesis zone in the CVD reactor confirmed macroscopic uniformity (**Figure S6**). This established that large-area high-quality graphene, needed for synthesizing pinhole-free membranes, can be prepared in large area CVD furnace by developing techniques to treat cheap Cu.

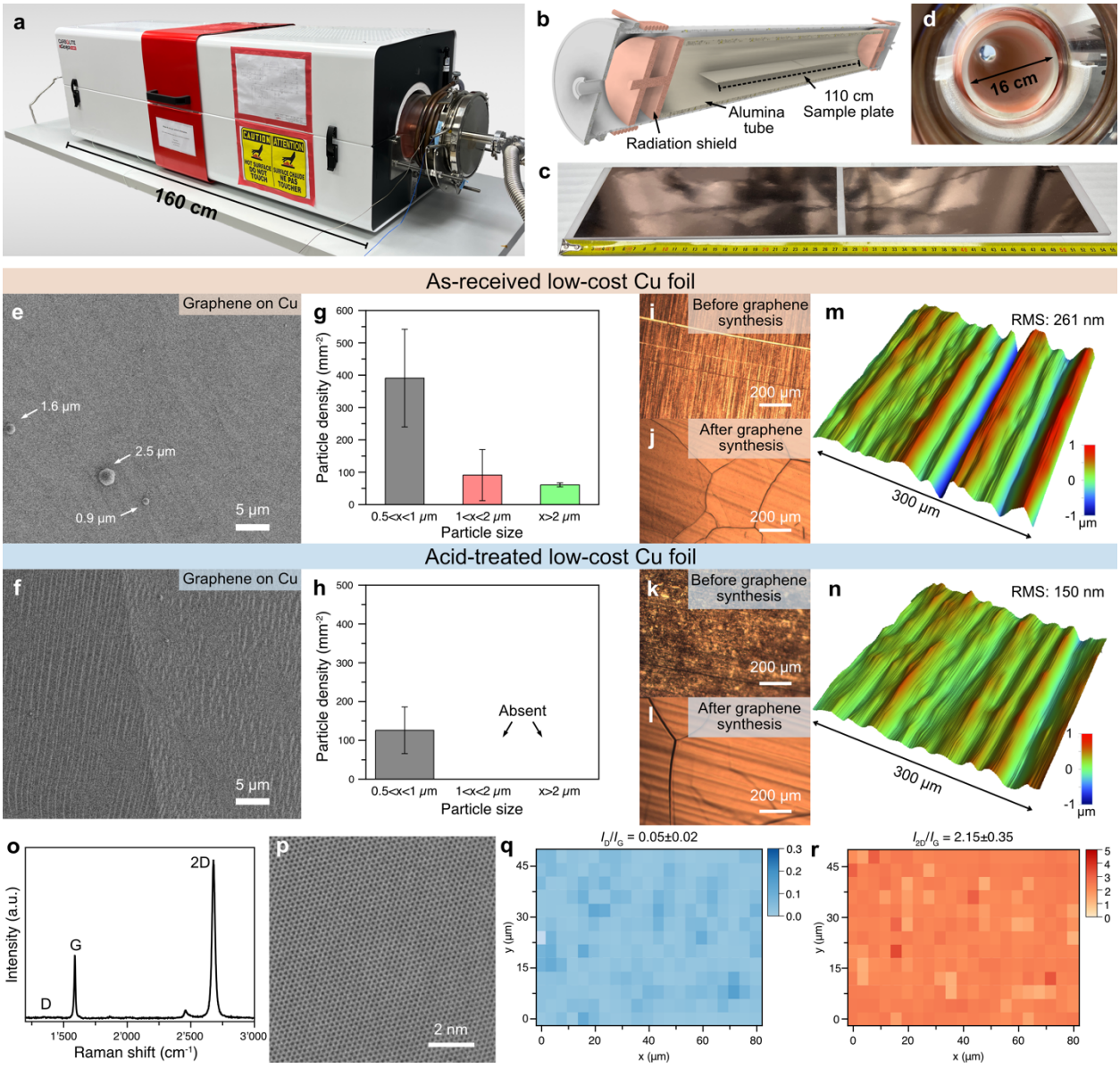

Figure 1. Synthesis of large-area graphene on low-cost Cu. a, A homebuilt CVD reactor for the synthesis of large-area graphene. **b,** Three-dimensional cross-section model of the reaction chamber equipped with radiation shields, an alumina tube, and a 110 cm long sample plate inside the heating zone. **c,** two 11 × 26 cm^2 single-layer graphene coupons synthesized in a single batch in the CVD reactor. **d,** the side view of the CVD reactor hosting a 16 cm in diameter alumina tube. **e-h,** SEM images of graphene surface grown on as-received (**e**) and acid-treated (**f**) Cu foil and the corresponding contamination particle density (**g, h**). **i-n,** Optical microscope images of as-received (**i, j**) and acid-treated (**k, l**) Cu foil before (**i, k**) and after graphene growth (**j, l**). Profilometry mapping images of as-received (**m**) and acid-treated (**n**) Cu foil after graphene

growth. **o,** Raman spectrum of graphene transferred on Si/SiO_2 wafer. **p,** AC-HRTEM image of single-layer graphene synthesized in this work. **q,r,** Raman mappings of *D* and *G* peak intensity ratio (I_D/I_G, **q**) and *2D* and G peak intensity ratio (I_{2D}/I_G, **r**) across an area of 48 × 80 μm^2.

Scalable incorporation of CO_2-selective pores in graphene

Oxidation of graphene in an O_3 flow leads to the formation of energy-minimizing O-clusters on graphene.[44,45] These clusters yield a pore at their core upon gasification.[46] We recently reported a simplified process of decoupling pore nucleation and expansion involving exposing graphene to O_3 followed by heat treatment or light exposure.[8,46,47] However, this approach has been limited to preparing small coupons. Implementing this concept for large-area PG requires developing a large-area reactor with a uniform reaction zone and the development of a dedicated protocol for incorporating uniform pores.

A 12-cm-diameter tubular reactor was implemented to fabricate a large-area PG (**Figure 2a**, experimental setup shown in **Figure S7**). This reactor could house an 11 cm wide and 55 cm long graphene coupon. The reactor was connected to an O_3 generator, yielding 8% O_3 in O_2. An evacuation and gas delivery system was designed to rapidly exchange the gas environment (argon (Ar), hydrogen (H_2), O_3) and to attain control over the reaction time. Several critical steps were identified and implemented in sequence. These are the removal of atmospheric contaminations on graphene, oxidation of graphene, gasification for pore generation, and finally, reduction of CuO formed during the O_3 exposure step. The corresponding conditions are detailed in **Figure 2b**.

Atmospheric contaminations deposit on the graphene surface when it is stored. If not removed, they hinder the oxidation of graphene. More importantly, depending on the coverage of contaminations, they make it challenging to achieve reproducible results. We found it to be an extremely critical step. Therefore, graphene was cleaned by heating under a reducing atmosphere of H_2/Ar mixture at 600 °C. While a lower temperature (500 ºC) was also effective, improved reproducibility was observed when heating to at least 600 ºC. Storage of CVD graphene also tends to generate CuO on the Cu foil, which makes the surface rough.[48] Heating under a reduced atmosphere helped smoothen the surface (Figure S8). This step was also crucial to obtain a smooth Cu/graphene surface, which was important for successful membrane fabrication. It should be noted that this step can be avoided when pore formation is implemented immediately after the synthesis of graphene.

For oxidation, the reactor temperature was lowered to the oxidation temperature, and the H_2/Ar atmosphere was exchanged with O_3. Samples were exposed to O_3 for a given period of time, after which they were cooled down to room temperature. O-clusters are formed on graphene during this step. The extent of oxidation was increased by either increasing the reaction time, temperature, or O_3 velocity (the latter discussed in the last section). To incorporate pores in the O-cluster, the oxidation with O_3 was stopped, and the reactor was heated to 150 ºC to facilitate the gasification of the clusters.

We observed that the oxidation step also resulted in the oxidation of Cu foil, which could be easily identified by a change in color to an intense red-orange (**Figure 2c, d**). This increased the foil's surface roughness, making graphene transfer challenging. Therefore, a reduction step was implemented at 600 ºC.

Pore incorporation in PG is indicated by a monotonic increase in I_D/I_G to 1.38±0.08 when the oxidation temperature was increased from 40 to 90 ºC (**Figure 2e**). The intensity of the 2D peak decreased as a function of oxidation consistent with the formation of high-density O-clusters, which makes graphene nanocrystalline. As oxidation progressed, an obvious *D'* peak appeared on the shoulder of the *G* peak with a *D'/G* peak ratio higher than 0.8, which confirmed the formation of carbon vacancies in graphene. This was also confirmed by gas permeation studies (see next section).

The Ramam mapping (20 × 40 μm^2) of I_D/I_G from the oxidized sample shows that oxidation was uniformly implemented at this length scale (**Figure 2f**). A systematic study of the mass transfer led to uniform oxidation in the entire oxidation zone (see section on mass transfer). Overall, the novel reactor allowed the realization of oxidation of large graphene coupons (500 cm^2) to form large-area PG. This establishes that large-area PG can be prepared uniformly by carefully designing a scale-up oxidation reactor.

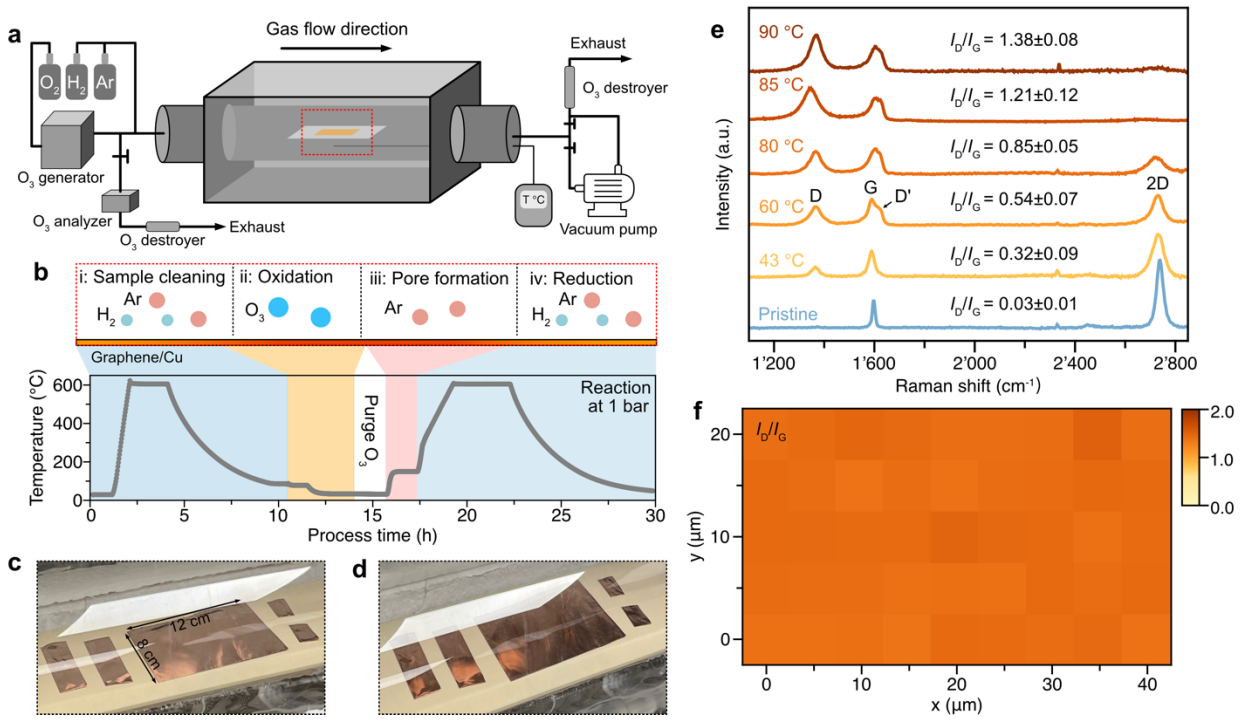

Figure 2. Scaled-up reactor for pore incorporation in graphene. a, Schematic illustration of the ozone functionalization setup. **b,** Oxidation schemes with corresponding temperature profiles used in the process. **c,d,** Photos of graphene samples before (**c**) and after oxidation (**d**). **e,** Raman spectra of graphene under various temperatures for oxidation. The spectra have been normalized to the *G* band intensity. **f,** Raman mapping of *D/G* peak intensity ratio of graphene oxidized at 90 ℃ across an area of 20 × 40 μm^2.

Crack-free transfer of large-area graphene to porous support

The MRF approach has been reported to address the crack formation in graphene during its transfer (**Figure S9**). While centimeter-scale membranes have been reported, the success rate has been low (10-20%) from stress generated in the film during wet-chemical etching of the film where the film is floated. To address this issue, we developed a facile transfer strategy involving a novel membrane module architecture (**Figure 3a, b**). This involved coating an MRF (PTMSP) on PG with a target thickness close to 1 μm (**Figure 3c**). The resulting Cu/PG/MRF was placed on a porous membrane support (polyethersulfone (PES), ~0.2 μm pores, **Figure 3d**) resting on a macroporous stainless steel (SS, **Figure 3e**) mesh. Step-by-step assembly of the module with a stacking order of Cu/PG/MRF/PES/SS mesh is illustrated in **Figure 3f**. The module was sealed by two rubber gaskets (**Figure 3b**) and was compressed by two cover plates (**Figure 3f, panels i and ii**).

The stacking order, Cu/PG/MRF/PES/SS mesh, exposes Cu foil on one side of the module, allowing one to etch and remove Cu directly from the assembled module. This effectively eliminated the need to float graphene. After sealing the module, the exposed Cu was placed in contact with a cell hosting a Cu etchant (1 M $FeCl_3$, **Figure 3f, panel iii**). During etching, PG reinforced by MRF was secured in the module. The thickness of MRF film played a crucial role. It was optimized as a function of the concentration of the PTMSP solution in toluene and spin-coating speed (**Figure S10**). A 1.2-µm-thick MRF film significantly improved the transfer of graphene. This is mainly because it allows residual SiO_x contaminants (< 1 µm in size) to be covered on graphene.

Optical microscope (**Figure 3g**) and SEM images (**Figure 3 h, i**) of the graphene surface exposed after removing Cu reveal the absence of any visible cracks. The reproducibility of this transfer strategy was probed by cutting a ~8 × 12 cm^2 graphene coupon (**Figure 3j**) into 24 pieces of 2 × 2 cm^2 coupons (**Figure 3k**) and fabricating membranes from each coupon (**Figure 3l**). An unsuccessful transfer typically leaves yellow residues on the white PES support because the Cu etchant ($FeCl_3$) penetrates the broken graphene (**Figure S11**). This is a useful and quick method to check the success of the transfer. We did not observe the yellow stain in these samples, indicating a successful transfer. Selective gas permeation from all membranes confirmed that graphene transfer's success rate was 100% (**Table S2**). The variation in CO_2 permeance in these samples is attributed to non-optimized O_3 velocity for these samples (see the next section).

The simple design of this module allowed the upscaling of the membrane element. However, the circular disk design of the above module limits the ability to achieve the practical cross-flow configuration. Therefore, larger decimeter-scale modules were designed by including cross-flow permeation channels (**Figure 4**). The membrane stacking order and Cu etching strategy were identical (**Figure 4a**). The module consisted of a symmetrical body frame and two identical cover plates to pack two 5 cm^2-sized membrane elements in a single module to increase the packing density. A cross-flow channel was created using slits on the side of the module (**Figure 4b).** Cu foil in the assembled module could be removed by flowing the etchant through the cross-flow slits (**Figure 4c**). This exposed graphene and generated a feed channel for gas permeation experiments. The cover plate on both sides had a central opening serving as a permeate window. This module could be further scaled into a larger one capable of hosting two 5 × 10 cm^2 membrane elements

(**Figure 4d**). Detailed pictures of a step-by-step assembly are shown in **Figures S12 and S13**. No yellow stain was observed in the transfer to this large module, which indicated a successful transfer.

The integrity of the graphene membranes transferred directly in the module was examined by gas permeation studies (setup shown in **Figure S14**). As-synthesized CVD graphene, without the oxidation step, yielded a low CO_2 permeance of 29 GPU with a CO_2/N_2 ideal selectivity of 15.6, consistent with the literature on intrinsic vacancy defects in graphene, confirming that cracks were avoided during transfer (**Table S3**). Successful crack-free transfer was also obtained from as-synthesized graphene transferred to the 5 cm^2 and 50 cm^2 cross-flow modules (**Table S3**). This establishes the robustness of this novel crack-free transfer approach in preparing large-area PG membranes.

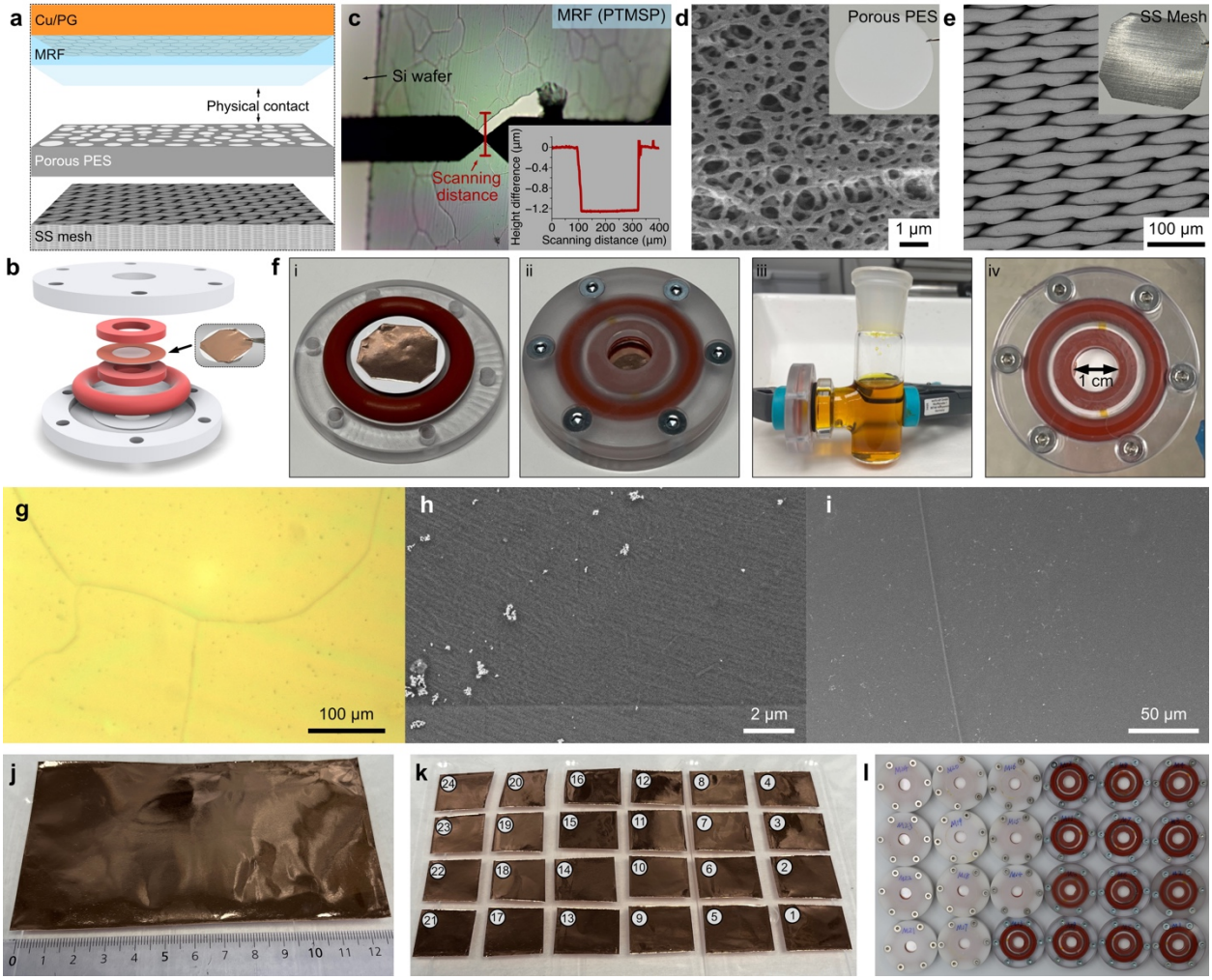

Figure 3. Crack-free direct transfer of graphene inside membrane module. a,b, Schematic illustration of graphene transfer strategy (**a**), and the architecture of the membrane module (**b**). **c,** Optical microscope image of the MRF transferred on a Si/SiO_2 wafer. The inset shows the film thickness characterization. **d,e,**

SEM images of commercial polyethersulfone (PES) support (**d**) and stainless steel (SS) mesh (**e**). The insets are pictures of the two supports. **f,** Pictures of stacked membrane assembly hosting Cu/PG/MRF/PES/SS mesh (**panels i and ii**), etching setup for Cu (**panel iii**), and as-prepared graphene membrane module after etching Cu foil **(panel iv**). **g-i,** Optical (**g**), and SEM (**h, i**) images of graphene surface after removal of Cu. **j-k,** A ~8 × 12 cm^2 graphene coupon (**j**) is cut into 24, 2 × 2 cm^2 small coupons (**k**). **l,** All 24 coupons in panel (**j**) lead to successful 1 cm-scale membranes. Half of the membrane modules were assembled with transparent cover plates to reveal the sealing.

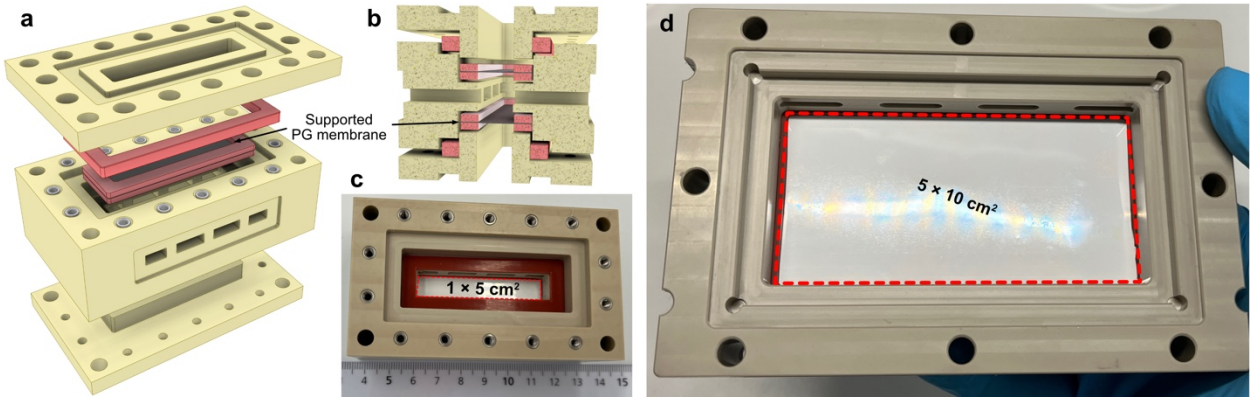

Figure 4. Graphene membranes prepared in large-area cross-flow modules. a,b, Three-dimensional model of the upgraded membrane module architecture (**a**), and the corresponding cross-section view showing the cross-flow slits (**b**). **c,d,** Photos of successfully prepared 1 × 5 cm^2 (**c**) and 5 × 10 cm^2 graphene membranes (**d**).

Reaction kinetics vs mass transfer in oxidation reactor

Oxidation of graphene was studied as a function of reaction kinetics (temperature, oxidation time), and mass transfer (ozone velocity). To understand the effect of reaction conditions on graphene porosity, the gas transport resistance model (**Supplementary Note S1, Table S2, S4, and S5**)[49] was used to extract permeance from the graphene layer. For PG membranes, the increase in porosity due to oxidation was indicated by an obvious increase in gas permeance compared to the membranes based on as-synthesized graphene (colored data points in **Figure 5a**).

A monotonic increase in CO_2 permeance as a function of reaction temperature for a fixed reaction time of 1 h could be observed (**Figure 5a**). An average increase in permeance from 1091 GPU to 2444 GPU was observed when the temperature increased from 85 to 90 ºC. The average CO_2/N_2 selectivity increased from 20.2 to 22.8, respectively. This favorable increase in CO_2 permeance, as well as CO_2/N_2 selectivity, can be attributed to a higher density of O clusters achieved at an elevated reaction temperature, given that cluster nucleation follows an energy barrier[46] and is consistent with the literature on millimeter-scale PG membranes.[46,47] Increasing the epoxidation time to 3 h at 85 ºC led to a further increase in CO_2 permeance of 2850 GPU with CO_2/N_2 selectivity of 19.3.

All previous studies on the oxidation of graphene have focused on reaction kinetics. Mass transfer limitation in the O_3-led oxidation reaction is important to consider because of the formation of an O_2 boundary layer next to graphene. The O_3 generator used in this study produces a dilute composition of O_3 (8% in O_2). Upon oxidation, a molecule of O_2 is produced per molecule of O_3, which further limits the concentration of O_3 near the graphene surface.[44] Computational fluid dynamics (CFD) simulations were performed using COMSOL to understand mass transfer. **Figure S15a** shows the simulated iso-surface plot of the gas velocity with an inlet flow rate of 2 l min^{-1} in the tubular reactor where a substrate holding Cu/graphene was placed. The highest velocity was near the center of the reactor. This is because of the small cross-sectional area of the gas delivery system relative to the reactor. The former was essentially a tube with an inner diameter of 2.2 cm. A boundary layer could be observed near the substrate where the gas velocity was significantly reduced. A two-dimensional (2D) plot of the gas velocity, 1 mm above the substrate, on a 6 × 16 cm area at the center of the substrate is shown in **Figure 5b**. The influence of the reactor geometry is apparent with varying gas velocity in different parts of the reactor. The gas flow was highest in the center and decreased at the edges of the reactor. The average gas velocity near graphene was 0.06 ± 0.04 cm s^{-1} ($\upsilon_{O_3,slow}$), indicating an uneven flow. A high standard deviation in velocity is not desired for obtaining uniformly porous graphene in scaled-up samples. To address this, a quartz semi-cylindrical block (12 cm in diameter) was placed in the reactor, occupying and blocking the bottom half of the unnecessary space for the ozone reaction. **Figure 5c** shows the tubular reactor hosting the semi-cylindrical block and a 55 cm-long graphene substrate plate. Attributing to the reduction in the cross-sectional area of the flow by the block, the gas develops a laminar flow at a short distance after the inlet (**Figure S15b**). A 2D plot of the gas velocity near graphene reveals a significantly uniform flow profile (**Figure 5d)**. The velocity increased three-fold to 0.17 ± 0.02 cm s^{-1} ($\upsilon_{O_3,fast}$). This led to a significant improvement in the porosity of graphene, reflected by a drastically improved CO_2 permeance. An average CO_2 permeance from the 1-cm-scale membranes of 13105 GPU and CO_2/N_2 selectivity of 15.1 could be achieved. Furthermore, the 50 cm^2 PG membrane in the 5 × 10 cm^2 cross-flow module yielded an attractive CO_2 permeance of 11799 and 8792 GPU, and CO_2/N_2 selectivity of 15.9 and 17.6, respectively (**Figure 5a and Table S5**). This shows that a carefully designed scaled-up reactor and transfer strategy allows one to achieve attractive performance from large-area graphene membranes.

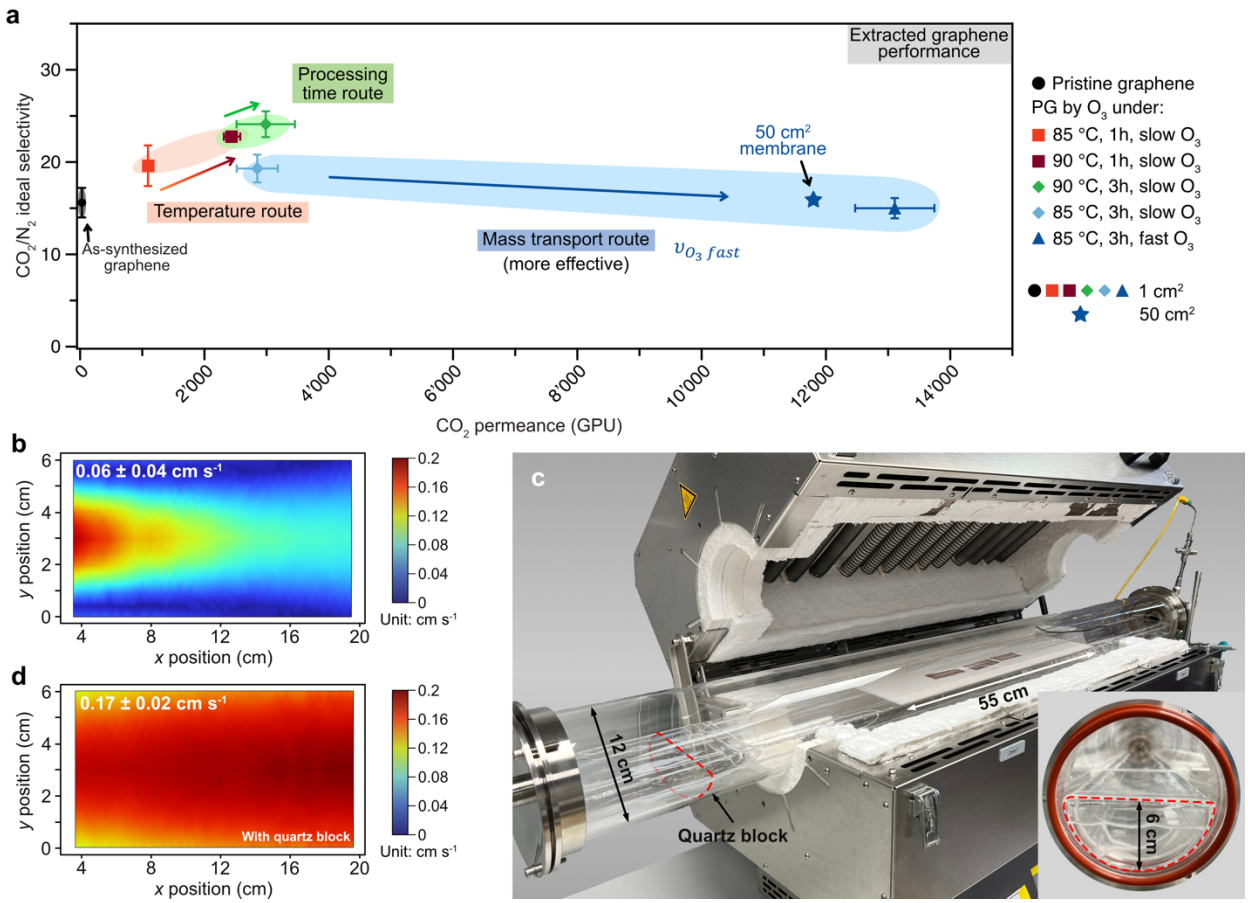

Figure 5. Optimization of oxidation kinetics and O_3 mass transfer. a, Gas permeation results of as-synthesized graphene (black) and PG (colored) membranes at 1 cm^2 and 50 cm^2-scale. The ozone oxidation was optimized by different reaction routes: temperature, processing time, and mass transport. The permeance of PG is extracted from the composite membrane using the transport resistance model (Supplementary Note S1).[49] **b,** COMSOL CFD simulation results from the unmodified reactor: extracted gas velocity 1 mm above the substrate in the middle of the reactor with a sample size of 6 × 16 cm^2. **c,** Picture of the modified ozone oxidation reactor hosting a quartz semi-cylindrical block (12 cm in diameter). The inset is the side view of the reactor with the quartz block. **d,** COMSOL CFD simulation results from the modified reactor at the same sample position in **b.**

Conclusion

Over a decade, the development of atom-thin graphene membranes has been limited by the lack of a scalable and reproducible membrane preparation method. This work shows that graphene membranes can be scaled up, that too with reduced cost and attractive performance in the important application of carbon capture. We address three key challenges: developing high-quality graphene and membranes from low-cost Cu foil, scaling up a reactor that allows the generation of porosity uniformly, and developing a transfer technique that allows the realization of a 50-cm^2-sized

graphene membrane in the cross-flow module. The reported method obtained an unprecedented near 100% success rate, which will allow a rapid proliferation of this technology. The methods discussed here, especially the use of low-cost Cu foil and the importance of mass transfer of O_3 in the oxidation of graphene, will soon form the basis for the roll-to-roll production of porous graphene membranes at a low cost. The rapidly growing field of two-dimensional porous materials will likely adopt the novel floating-free transfer approach introduced here.

Methods

Synthesis of CVD graphene

Commercial copper foils (Table S1) were pre-treated with nitric acid (4 wt%) for 10 min to remove the surface contamination. Cu foils were washed with deionized water four times and stored in isopropanol before use. A customized CVD furnace (Carbolite, TS1/3-1200, heating zone 1.2 m) hosting a quartz tube and an alumina tube (Zibo Highlion New Material Co., Ltd) was built for graphene synthesis.

The synthesis protocol of CVD graphene followed the previous reports.[23,25,43] First, the Cu foil was treated at 1020 ℃ for 2 h under 1 bar CO_2 flow to remove surface carbonaceous contaminations. After exchanging the gas to Ar and H_2 with a flow rate of 500 and 50 sccm, respectively, the furnace was slowly heated to 1065 ℃ and the temperature was maintained for 3 h. The graphene synthesis was conducted at 1020 ℃ using 9 sccm of CH_4 and 3 sccm of H_2 under a pressure of 180 mTorr for 30 min. Detailed temperature and pressure profiles are shown in Figure S1.

Characterization of graphene

SEM imaging was conducted on a FEI Teneo scanning electron microscope at a working voltage of 1 kV. Graphene grown on Cu foil was directly imaged without further surface treatment. EDX was used to analyze the elements of the contamination particles. The macroscopic surface features of the Cu substrate and graphene were obtained from an optical microscope. Graphene sample roughness and polymer thickness measurements were performed on Bruker DektakXT stylus profilometer with a 2-µm stylus radius and 3 mg force. The data was processed by Bruker Vision

64 v5.51 software. AC-HRTEM imaging of graphene was realized on a ThermoFischer Titan Themis operated at 80 kV.

The quality of graphene was examined by Reinshow inVia^{TM} micro-Raman spectroscope. 457 nm laser was used to characterize graphene grown on the Cu substrate, and 532 nm laser was used for graphene transferred on a Si/SiO_2 wafer by the conventional wet transfer method. The peak intensity ratio was analyzed by fitting the spectra using least-squares curve fitting tools in MATLAB.

Oxidation of graphene in ozone

O_3-based oxidation of graphene was conducted in a tubular furnace (Nabertherm, 90 cm heating zone) hosting a 1.5 m long, 12 cm in diameter quartz tube (Figure S6). O_3 (2 l min^{-1}) was produced from a commercial O_3 generator (Absolute Ozone, Atlas 60) and stabilized for at least 30 min to reach 8 wt% (O_3/O_2) as analyzed by a O_3 monitor (2B Technologies, Model 106-H).

Transfer of graphene to membrane module

PG was first spin-coated with a layer of PTMSP (abcr GmbH). The solution was prepared by dissolving 3 g of PTMSP into 97 g of toluene and subsequently centrifuged to remove the impurities. The spin coating was carried out at 1000 rpm for 1 min in a large-area spin coater (Laurell Technologies Corporation, WS-650Hz-15NPPB). After drying overnight, the polymer-reinforced graphene was first attached to a commercial porous PES support (Haining, China, 0.1 mm thickness, 0.22 μm pore opening) film, then to SS meshes (TWP), and the assembly was sealed into the custom-made membrane module described in this work. $FeCl_3$ (1 M) solution was used to etch the Cu foil, followed by a cleaning using HCl (1 M) solution and deionized (DI) water.

Gas permeation measurement

Single-component gas permeation measurement was performed using a constant-volume, variable-pressure method. The scheme and pictures of the experimental setup are shown in Figures S13 and S14. Before the measurement, the membrane module was sealed with an impermeable Cu foil to measure the system leak rate. The leak rate was negligible (~ 1 GPU). The permeance was calculated by the following equation:

$$Permeance_i = \frac{J_i}{A\Delta P_i} = \frac{V}{ART\Delta P_i}\frac{dP}{dt} \quad \text{(eq. 1)}$$

where J_i is the flux of the gas component i, A is the membrane area, R is the ideal gas constant, ΔP_i is the pressure difference of gas component i from the feed and the permeate side, and $\frac{dP}{dt}$ is the pressure change in the constant permeate volume. Different feed gases were used to probe the permeation performance of the membrane. For each gas measurement, a sufficient gas flow controlled by a mass flow controller (MFC) was supplied to the feed side of the membrane. For membranes that have a high flux, the permeate flux was measured using a bubble flow meter according to the following equation:

$$Permeance_i = \frac{J_i}{A\Delta P_i} = \frac{1000}{24.77 A \Delta P_i}\frac{dV}{dt} \quad \text{(eq. 2)}$$

where $\frac{dV}{dt}$ is the permeate flow rate (ml s^{-1}) at the ambient condition (25 °C and 1 bar). A forced air convection oven was equipped to measure the gas permeance at elevated temperatures. All membrane data were collected after heating the membrane to 130 °C for 1 h followed by cooling to 25 ºC. This allowed the removal of any atmospheric contaminations in the sample.

Computational fluid dynamics (CFD) simulation

CFD simulations on the gas profile in the tubular furnace were performed using a COMSOL Multiphysics®6.1 package. The model geometry was created in the software as shown in Figure S14. O_2 was selected as the fluid material. A laminar flow study was applied to the model, with a gas inlet and outlet specified on the left and right ends of the reactor. Other domains of the model were all defined as wall boundaries. The boundary condition for the inlet was set as a fully developed flow with a flow rate of 2 l min^{-1}, and that for the outlet was set as a static pressure of 0 Pa. The results were analyzed by COMSOL.

Acknowledgment

We acknowledge GAZNAT for funding this work. M.R. acknowledges Bridge Proof of Concept for funding the work on optimizing low-cost Cu foil. L.S.B., D.B., and K.B. acknowledge the host institute, EPFL, for funding aspects of the project related to characterization and support optimization. We thank the EPFL mechanical workshop for fabricating membrane modules.

Data availability

The data supporting the findings of this study are available within the article and Supplementary Information file.

References:

1. Drahushuk, L. W. & Strano, M. S. Mechanisms of gas permeation through single layer graphene membranes. *Langmuir* **28**, 16671–16678 (2012).

2. Koenig, S. P., Wang, L., Pellegrino, J. & Bunch, J. S. Selective molecular sieving through porous graphene. *Nat. Nanotechnol.* **7**, 728–732 (2012).

3. O'Hern, S. C. *et al.* Selective molecular transport through intrinsic defects in a single layer of CVD graphene. *ACS Nano* **6**, 10130–10138 (2012).

4. Cohen-Tanugi, D. & Grossman, J. C. Water desalination across nanoporous graphene. *Nano Lett.* **12**, 3602–3608 (2012).

5. Li, H. *et al.* Ultrathin, molecular-sieving graphene oxide membranes for selective hydrogen separation. *Science* **342**, 95–98 (2013).

6. Huang, S. *et al.* Single-layer graphene membranes by crack-free transfer for gas mixture separation. *Nat. Commun.* **9**, 1–11 (2018).

7. He, G. *et al.* High-permeance polymer-functionalized single-layer graphene membranes that surpass the postcombustion carbon capture target. *Energy Environ. Sci.* **12**, 3305–3312 (2019).

8. Huang, S. *et al.* Millisecond lattice gasification for high-density CO_2- and O_2-sieving nanopores in single-layer graphene. *Sci. Adv.* **7**, eabf0116 (2021).

9. Soo, X. Y. D. *et al.* Advancements in CO_2 capture by absorption and adsorption: A comprehensive review. *J. CO_2 Util.* **81**, 102727 (2024).

10. Mota-Martinez, M. T., Hallett, J. P. & Dowell, N. M. Solvent selection and design for CO_2 capture – how we might have been missing the point. *Sustain. Energy Fuels* **1**, 2078–2090 (2017).

11. Sholl, D. S. & Lively, R. P. Seven chemical separations to change the world. *Nature* **532**, 435–437 (2016).

12. Darunte, L. A., Walton, K. S., Sholl, D. S. & Jones, C. W. CO_2 capture via adsorption in amine-functionalized sorbents. *Curr. Opin. Chem. Eng.* **12**, 82–90 (2016).

13. Du, N., Park, H. B., Dal-Cin, M. M. & Guiver, M. D. Advances in high permeability polymeric membrane materials for CO_2 separations. *Energy Environ. Sci.* **5**, 7306–7322 (2012).

14. Han, Y. & Ho, W. S. W. Polymeric membranes for CO_2 separation and capture. *J. Membr. Sci.* **628**, 119244 (2021).

15. Varoon Agrawal, K. *et al.* Dispersible exfoliated zeolite nanosheets and their application as a selective membrane. *Science* **334**, 72–75 (2011).

16. Rangnekar, N., Mittal, N., Elyassi, B., Caro, J. & Tsapatsis, M. Zeolite membranes – a review and comparison with MOFs. *Chem. Soc. Rev.* **44**, 7128–7154 (2015).

17. Chen, G. *et al.* Zeolites and metal–organic frameworks for gas separation: the possibility of translating adsorbents into membranes. *Chem. Soc. Rev.* **52**, 4586–4602 (2023).

18. Babu, D. J., He, G., Villalobos, L. F. & Agrawal, K. V. Crystal engineering of metal–organic framework thin films for gas separations. *ACS Sustain. Chem. Eng.* **7**, 49–69 (2019).

19. Li, H., Dilipkumar, A., Abubakar, S. & Zhao, D. Covalent organic frameworks for CO_2 capture: from laboratory curiosity to industry implementation. *Chem. Soc. Rev.* **52**, 6294–6329 (2023).

20. Patel, H. A. *et al.* Unprecedented high-temperature CO_2 selectivity in N_2-phobic nanoporous covalent organic polymers. *Nat. Commun.* **4**, 1357 (2013).

21. Huang, S. *et al.* Ultrathin carbon molecular sieve films and room-temperature oxygen functionalization for gas-sieving. *ACS Appl. Mater. Interfaces* **11**, 16729–16736 (2019).

22. Rungta, M. *et al.* Carbon molecular sieve structure development and membrane performance relationships. *Carbon* **115**, 237–248 (2017).

23. Li, X. *et al.* Large-area synthesis of high-quality and uniform graphene films on copper foils. *Science* **324**, 1312–1314 (2009).

24. Polsen, E. S., McNerny, D. Q., Viswanath, B., Pattinson, S. W. & John Hart, A. High-speed roll-to-roll manufacturing of graphene using a concentric tube CVD reactor. *Sci. Rep.* **5**, 10257 (2015).

25. Bae, S. *et al.* Roll-to-roll production of 30-inch graphene films for transparent electrodes. *Nat. Nanotechnol.* **5**, 574–578 (2010).

26. Li, X. *et al.* Large-area graphene single crystals grown by low-pressure chemical vapor deposition of methane on copper. *J. Am. Chem. Soc.* **133**, 2816–2819 (2011).

27. Ramasubramanian, K., Verweij, H. & Winston Ho, W. S. Membrane processes for carbon capture from coal-fired power plant flue gas: A modeling and cost study. *J. Membr. Sci.* **421–422**, 299–310 (2012).

28. Merkel, T. C., Lin, H., Wei, X. & Baker, R. Power plant post-combustion carbon dioxide capture: An opportunity for membranes. *J. Membr. Sci.* **359**, 126–139 (2010).

29. Yuan, Z., Benck, J. D., Eatmon, Y., Blankschtein, D. & Strano, M. S. Stable, temperature-dependent gas mixture permeation and separation through suspended nanoporous single-layer graphene membranes. *Nano Lett.* **18**, 5057–5069 (2018).

30. Cheng, P. *et al.* Facile size-selective defect sealing in large-area atomically thin graphene membranes for sub-nanometer scale separations. *Nano Lett.* **20**, 5951–5959 (2020).

31. Zhang, D. *et al.* Bioinspired large-area atomically-thin graphene membranes. *Adv. Funct. Mater.* **34**, 2307419 (2024).

32. Yamada, Y. *et al.* Subnanometer vacancy defects introduced on graphene by oxygen Gas. *J. Am. Chem. Soc.* **136**, 2232–2235 (2014).

33. Wang, X. & Dai, H. Etching and narrowing of graphene from the edges. *Nat. Chem.* **2**, 661–665 (2010).

34. Agrawal, K. V. *et al.* Fabrication, pressure testing, and nanopore formation of single-layer graphene membranes. *J. Phys. Chem. C* **121**, 14312–14321 (2017).

35. Kidambi, P. R. *et al.* A scalable route to nanoporous large-area atomically thin graphene membranes by roll-to-roll chemical vapor deposition and polymer support casting. *ACS Appl. Mater. Interfaces* **10**, 10369–10378 (2018).

36. Cheng, C., Iyengar, S. A. & Karnik, R. Molecular size-dependent subcontinuum solvent permeation and ultrafast nanofiltration across nanoporous graphene membranes. *Nat. Nanotechnol.* **16**, 989–995 (2021).

37. Reina, A. *et al.* Large area, few-layer graphene films on arbitrary substrates by chemical vapor deposition. *Nano Lett.* **9**, 30–35 (2009).

38. Suk, J. W. *et al.* Transfer of CVD-grown monolayer graphene onto arbitrary substrates. *ACS Nano* **5**, 6916–6924 (2011).

39. Lin, Y.-C. *et al.* Clean transfer of graphene for isolation and suspension. *ACS Nano* **5**, 2362–2368 (2011).

40. Hsu, K.-J. *et al.* Graphene membranes with pyridinic nitrogen at pore edges for high-performance CO_2 capture. *Nat. Energy* **9**, 964–974 (2024).

41. Lee, W.-C. *et al.* Centimeter-scale gas-sieving nanoporous single-layer graphene membrane. *J. Membr. Sci.* **618**, 118745 (2021).

42. Lisi, N. *et al.* Contamination-free graphene by chemical vapor deposition in quartz furnaces. *Sci. Rep.* **7**, 9927 (2017).

43. Rezaei, M., Li, S., Huang, S. & Agrawal, K. V. Hydrogen-sieving single-layer graphene membranes obtained by crystallographic and morphological optimization of catalytic copper foil. *J. Membr. Sci.* **612**, 118406 (2020).

44. Vahdat, M. T. *et al.* Mechanistic insights on functionalization of graphene with ozone. *J. Phys. Chem. C* **127**, 22015–22022 (2023).

45. Lee, G., Lee, B., Kim, J. & Cho, K. Ozone adsorption on graphene: Ab initio study and experimental validation. *J. Phys. Chem. C* **113**, 14225–14229 (2009).

46. Huang, S. *et al.* In situ nucleation-decoupled and site-specific incorporation of Å-scale pores in graphene via epoxidation. *Adv. Mater.* **34**, 2206627 (2022).

47. Bondaz, L. *et al.* Selective photonic gasification of strained oxygen clusters on graphene for tuning pore size in the Å regime. *JACS Au* **3**, 2844–2854 (2023).

48. Zhou, F., Li, Z., Shenoy, G. J., Li, L. & Liu, H. Enhanced room-temperature corrosion of copper in the presence of graphene. *ACS Nano* **7**, 6939–6947 (2013).

49. Fu, Q. *et al.* A novel cross-linked nano-coating for carbon dioxide capture. *Energy Environ. Sci.* **9**, 434–440 (2016).